Experimental Investigation of Unsteady Fan Flow Interaction with Downstream Struts

W. F. Ng,* W. F. O'Brien,† and T. L. Olsen‡
Virginia Polytechnic Institute and State University, Blacksburg, Virginia

The detailed unsteady pressure field produced on the rotor blades by interaction with downstream struts was investigated using blade-mounted, high-frequency pressure transducers. The experiments were carried out in a single-stage, low-speed, axial-flow fan, the arrangement of which was similar to that found in the fan casings of turbofan aircraft engines. Stationary pressure probes were also used to map the flowfield. The results of the measurements of fluctuating pressures are presented for midspan and 85% span for both the suction and pressure surfaces of the rotor blades for several positions of the downstream struts and for two flow coefficients (C_x/U_T). Unsteady lift and moment are calculated by integrating the pressures measured by the blade-mounted transducers. In addition, a sequence of instantaneous fluctuating pressure distributions on the blade surfaces presented over time shows how the rotor is influenced by the potential effect of the struts. The strut is shown to produce an effect on the unsteady pressure field on the rotor blades. This unsteady effect exceeds that due to the stator at design rotor/stator/strut spacing, but falls off rapidly as the struts are moved downstream. However, results from stationary probe measurements show that the presence of the downstream strut has no measurable effect on the aerodynamic performance of the rotor.

Nomenclature

C_{p_t} = nondimensionalized total pressure coefficient
C_{p_s} = nondimensionalized static pressure coefficient
C_x = axial velocity
ΔC_ℓ = nondimensionalized unsteady lift coefficient
ΔC_m = nondimensionalized unsteady moment coefficient
ΔC_p = nondimensionalized unsteady pressure coefficient
P_t = total pressure
P_s = static pressure
U_T = blade tip speed
ρ = air density

Motivation and Introduction

THE impetus for the present work came from a fan duct flow problem found in modern aircraft gas turbine engines. The interaction between blade and vane rows of axial-flow turbomachines is a matter of increasing concern as techniques for flow analysis mature. Three-dimensional computer codes including viscous effects provide for near-optimum design of blade and vane rows. The understanding and tailoring of the flow considering the influence of rotating and stationary blade rows upon one another is one of the next steps to improve machine performance.

The present paper addresses flow interaction between a fan, a downstream set of stator vanes, and a following strut row. Results from an experiment in a rig configured to represent the bypass flow path in turbofan engines are presented and interpreted. The experiment involves the flow disturbance field caused by relatively large and bulky struts located downstream of both the fan and fan exit guide vanes (stators). These struts bifurcate the fan duct and house the engine attachment structure, plumbing, and control fittings. The potential field distortion due to such struts, which normally extends upstream through an adjacent stator row, produces an unsteady excitation force on the upstream rotor or fan. The possibility of vibratory fatigue on the rotor blade due to the presence of such an excitation must therefore be seriously considered. Fluctuating lift caused by flow unsteadiness over the fan airfoils is also a mechanism for noise generation and, thus, should be minimized as much as possible. Recently, there has been concern on the aerodynamic performance of the rotor under the influence of the downstream struts. Efficiency can be affected due to the close proximity of the strut to the rotor. This experimental program has been set up to investigate some of these phenomena.

Initially because of the vibratory fatigue problem, and more recently because of the effect on turbomachinery noise and also because of performance consideration, the fan rotor/strut interaction phenomenon has been examined by many investigators. On the analytical side, Rubbert et al.[1] used inviscid potential flow theory to examine screening the effect of the struts through stator modification. Barber and Weingold[2] adapted the Douglas-Neumann potential method to predict the steady, two-dimensional flowfield through multibody cascade geometries. O'Brien et al.[3] coupled a Douglas-Neumann potential flow solution with a time-marching code to model the rotor/stator/strut interaction. On the experimental side, Preisser et al.[4] and Woodward and Balombin[5] used a test engine and correlated blade-mounted transducer signals and far-field noise with the interaction of a rotor and downstream struts. Yokoi et al.[6] tested a two-stage fan with downstream struts and showed that the potential field of these struts could induce significant blade vibration in the upstream rotor.

In each of the above experimental investigations, only one or two pressure transducers were mounted on the rotor blades to measure the unsteady pressure fluctuations. Hence, it was not possible to integrate pressure distribution over the blade surfaces to give the unsteady lift and moment on the fan blades resulting from interaction with the downstream struts. Not only is such information useful for comparison with theoretical predictions, but it is a necessary part of a global integrated rotor response model. In addition, no data

Received May 16, 1986; presented as Paper 86-1870, at the AIAA 10th Aeroacoustics Conference, Seattle, WA, July 9–11, 1986; revision received Sept. 24, 1986.

*Assistant Professor, Department of Mechanical Engineering. Member AIAA.
†Professor, Department of Mechanical Engineering. Member AIAA.
‡Graduate Research Assistant, Department of Mechanical Engineering.

set exists in the literature that investigates the details of aerodynamic performance of the rotor under the influence of the downstream struts. The need to examine these topics prompted this study.

The paper begins with a description of the experiment, which includes a discussion of the basic dimensions used in the data analysis. Following this, the results of the experiments are presented. These include samples of the pressure fluctuations measured by the blade-mounted transducer and the unsteady lift and moment coefficients measured by integrating the pressure on the blade. A comparison is made between the magnitude of the unsteadiness caused by the rotor/strut interaction and rotor/stator interaction. In addition, instantaneous perturbation pressure distributions on the blade induced by the struts are presented in a time sequence. Finally, measurements using stationary pressure probes are presented to show the effect of the downstream struts on the aerodynamic performance of the rotor.

Experimental Facility and Technique

Low-Speed Compressor Facility

The research compressor was a modified General Electric model 5GDY34A1 axial-flow fan/dynamometer set, configured as a single-stage rotor and stator. A speed variator allowed speeds up to 3000 rpm. The rotor consisted of 24 RAF-6 propeller sections having a twist of 4 deg with a midspan stagger angle of 45 deg and an aspect ratio of 1.66. The stators were located 33 mm behind the trailing edge of the rotor. There were 37 stators with a hub-to-tip twist of 8 deg and a midspan 15 deg stagger angle. The stator had an aspect rtio of 1.58. Table 1 lists the major design and performance parameters of the compressor.

For the present investigation, a set of five struts was fabricated for installation downstream of the stator vanes. A NACA 0021 symmetrical airfoil profile was selected for the struts. Figure 1 shows the arrangement and angle settings of the rotor blades, stator vanes, and struts. Spaced evenly around the circumference, the struts are placed at a uniform moveable axial location. This test program used axial locations of 119, 140, 165, and 254 mm behind the rotor trailing edge, measured to the strut leading edge. They are correspondingly referred to as strut positions 1, 1.5, 2, and 3, with the additional position 0 (zero) indicating the absence of struts. The first strut position is closest to the stator and corresponds to that in an actual engine. This will be referred to as the design strut location in the following sections. The maximum distance (strut position 3) was set for a negligible difference with the no-strut case. A cubic plenum follows the discharge annulus, with an adjustable valve for airflow regulation leading to the long exhaust duct. More detailed information is given by Reimers.[7]

On-Rotor Pressure Measurement Technique

Measurement of on-rotor fluctuating pressures was taken by blade-mounted transducers. The transducers employed in the present investigation were Kulite model LQ-125-10, with 68 kPa full-scale pressure. Six transducers were located on the suction side of a rotor blade and another six were placed on the pressure side of the following blade. The transducers were placed along the chordline at the midspan. A correction for phase shift is applied to the data in the subsequent analysis to account for the phase difference between the pressure and suction surface data. A similar arrangement produced pressure measurements at the 85% span position. Locations of the transducers were 10, 25, 40, 55, 70, and 85% of the aerodynamic chord of the rotor blade, measured from the leading edge.

The thickness of the rotor blade permitted the milling of slots for embedding the transducers and wires in the blade. After mounting, the transducers and wires were held in place by silicon rubber filler material, smoothed to the original airfoil shape. The transducers measured the local static pressure on the airfoil surface through a port above the pressure-sensitive diaphragm. The calculated frequency response for the port and the volume above the transducer was much greater than the frequencies of the disturbances produced by the 5 downstream struts (242 Hz) and by the 37 stator blades (1788 Hz). A previous investigation showed that the performance of the transducers was unaffected by the rotation of the rotor. The considerable temperature drift of the semiconductor transducers could not be compensated for completely. Therefore, the transducers were a.c. coupled and only the fluctuating portions of the pressures were measured.

Stationary Pressure Measurements

Stationary pressure and flow direction were measured with three United-Sensor three-hole probes. Probe A was placed 6.4 mm upstream of the rotor leading edge. Probes B and C were placed 6.4 and 113.0 mm, respectively, behind the rotor trailing edge. Probe C was located between the stator and the strut. The relative position of the probes is shown in Fig. 1. Stationary pressure measurements were taken at the midspan

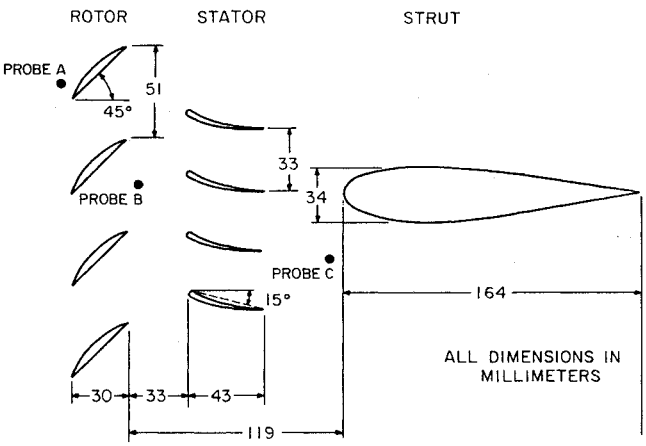

Fig. 1 Compressor cross section showing rotor/stator/strut spacing.

Table 1 Data for low-speed single-stage compressor rig

System parameters	
Operating speed	2900 rpm
Tip diameter of compressor	0.46 m
Approximate design point flow	3 m^3/s
Rotor blades	
Number of blades	24
Rotor blade airfoil	RAF-6, 12% thickness
Chord	42.3 mm
Span	70.1 mm
Midspan stagger angle	45 deg
Midspan solidity	0.84
Stator vanes	
Number of blades	37
Chord	44.0 mm
Span	70.1 mm
Vane turning angle	~ 30 deg
Midspan solidity	1.36
Struts	
Number of struts	5
Strut airfoil	NACA 0021
Chord	164.0 mm
Thickness	34.0 mm
Midspan circumferential spacing	0.25 m

and 85% span, with the downstream struts at position 1 and also with the downstream struts removed. Because of limitations in the experimental apparatus, circumferential variation in the flowfield between stator blades was not surveyed using probe B. Instead, the focus was on the circumferential distortion caused by the struts. Absolute flow angles measured from the axial direction, total pressures, and static pressures were measured while the struts were rotated circumferentially over 72 deg, in increments of 3 deg. This technique is equivalent to moving the probes in the circumferential direction to survey the nonuniform distortion caused by the struts. The probes were used with a Statham pressure transducer operating into a bridge amplifier for nulling and a slant manometer for pressure readings. The combined on-rotor and stationary pressure measurements provided a set of data containing the unsteady rotor response as well as the magnitude of flow disturbances producing the response.

Data Acquisition and Experimental Procedure

Instrumentation limitations allowed measurement of only the time-varying (a.c.) component of the fluctuating pressure. No absolute steady-state (d.c.) level of the pressure on the blade was recorded during the experiment. The signals from the on-rotor pressure measurements system and a signal recording the rotor position were simultaneously stored on an instrumentation recorder. All analog data recorded on tapes were digitized and transferred to the computer for digital analysis.

The compressor was operated at a rotational speed of 2900 rpm, corresponding to a rotor tip speed of 69.4 m/s. Test points were selected by adjusting compressor flow to flow coefficients C_x/U_T of 0.48 and 0.54, producing near-design-point and reduced rotor aerodynamic loading, respectively. (Here C_x is the axial velocity and U_T the blade speed at the tip.) The Reynolds number based on the rotor's midspan relative inlet velocity and rotor chord length is 1.8×10^5 for $C_x/U_T=0.48$. The reduced frequency based on rotor inlet relative velocity and the rotor half-chord is calculated to be 0.09 and 0.68 for the strut and the stator, respectively.

Treatment of Dimensions

The data are presented in nondimensional form. The significant units of time are the digitization sample increments and the duration of one shaft revolution. The data are digitized such that one shaft revolution contains 360 sample increments (independent of the fan speed), so that one increment may be related to 1 deg of the rotor angle. One revolution contains 360 deg and five equally spaced downstream struts occur every 72 deg. Therefore, all time axes are reported in degrees of rotor angle.

For spectral analysis of the data, the frequency axes are labeled in machine order, which is the first harmonic of rotor speed. The rotor shaft speed of 2900 rpm is equivalent to 48.33 Hz, which is defined as machine order one. Thus, the disturbance caused by five downstream struts equally spaced circumferentially will occur at the fifth machine order. Similarly, the disturbance caused by 37 stator blades will occur at the 37th machine order.

Distances along the rotor chord from the blade leading edge are nondimensionalized by rotor chord length. Rotor/strut axial spacing is nondimensionalized by strut thickness and is measured from the rotor trailing edge to the strut leading edge.

Fluctuating pressure, lift, and moment have also been nondimensionalized. At low rotational speed, the fluid can be assumed to be incompressible. Fluctuating pressure, available in pascals, is nondimensionalized by dynamic pressure to give a coefficient of pressure ΔC_p of

$$\Delta C_p = \frac{\text{fluctuating pressure}}{\frac{1}{2}\rho U_T^2}$$

Table 2 Summary of stationary pressure measurements

		Strut position 1			Strut removed		
C_x/U_T	Span, %	C_{p_t}	C_{p_s}	Angle, deg	C_{p_t}	C_{p_s}	Angle, deg
0.48	50	0.53	0.23	36	0.53	0.23	36
0.48	85	0.60	0.23	37	0.61	0.23	37
0.54	50	0.51	0.19	32	0.52	0.19	34
0.54	85	0.60	0.19	33	0.61	0.19	34

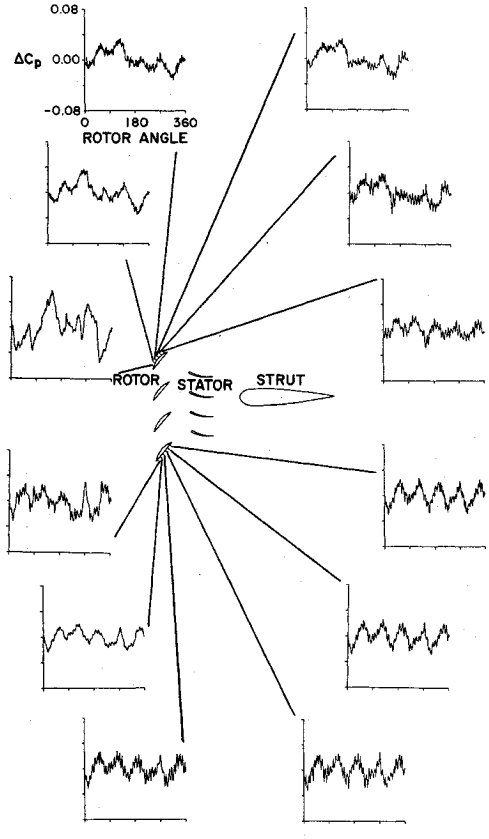

Fig. 2 Ensemble-averaged unsteady pressure data at the midspan, $C_x/U_T=0.48$.

where ρ is the density of air. Unsteady lift is computed in force per unit length of span, which is nondimensionalized by the dynamic pressure and rotor aerodynamic chord to give the fluctuating lift coefficient ΔC_ℓ. Similarly, unsteady moment in torque per length ΔC_m is nondimensionalized by dynamic pressure and chord length squared.

The stationary probe measurements are given in nondimensionalized total and static pressure coefficients where

$$C_{p_t} = \frac{P_t - P_{\text{atm}}}{\frac{1}{2}\rho U_T^2} \text{ and } C_{p_s} = \frac{P_s - P_{\text{atm}}}{\frac{1}{2}\rho U_T^2}$$

The absolute flow angles are reported in degrees and are measured from the axial direction.

Experimental Results and Discussion

Analysis Technique and Sample Data

As mentioned previously, because of instrumentation limitations, the steady part of the pressures on the blade suction and pressure surfaces cannot be determined. However, the fluctuating part can be isolated by referencing the data to zero over some large time period. This unsteady component is the subject of analysis and is used to give fluctuating pressure.

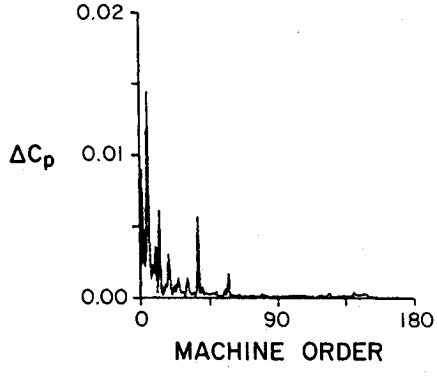

Fig. 3 Sample frequency spectrum of unsteady pressure data.

Ensemble averaging is used to reduce background fluctuation. The data are assumed to be stationary and periodic with a fundamental period of one rotor revolution. When many cycles of data are averaged point by point over time, random fluctuations are smoothed out in the resulting data set. Two hundred cycles are used for ensemble averaging with the equation

$$\bar{P}(\theta_k) = \sum_{i=1}^{N} P_i(\theta_k), \quad k = 1, 2, \ldots, 360$$

where N cycles (200) are averaged for each rotor angle θ_k and i is the number of the fan revolution. Figure 2 shows sample ensemble-averaged data plots for the midspan location $C_x/U_T = 0.48$ and for strut location 1. Fluctuating pressure levels are shown to the same scale. Each pattern repeats itself each full revolution. The 5/rev strut disturbance can be seen clearly. In addition, Fig. 2 shows the 37/rev stator disturbance superimposed on the pressure fluctuation. The pressure fluctuation on the suction surface is generally less well behaved, especially near the leading edge. This may be due to more turbulent flow patterns near a blade suction surface or possible flow separation on the suction side of the blade.

The frequency content of the pressure fluctuation is displayed by performing a digital fast Fourier transformation of a set of averaged data. Figure 3 shows a sample plot of the frequency spectrum for the ensemble-averaged data for the transducer on the pressure side at the midspan, $C_x/U_T = 0.48$, 10% chord, and strut location 1. Notable components appear at harmonics 1, 5, and 37, which correspond to the 1/rev background disturbance, the 5 downstream struts (rotor/strut interaction), and the 37 stator blades (rotor/stator interaction). The peak at a particular frequency on the spectrum corresponds to an average magnitude of the disturbance. The vertical axis in Fig. 3 is amplitude (not power or amplitude squared), such that the average peak-to-peak amplitude of the fluctuation at the 5/rev disturbance on Fig. 2 is the same as to twice the amplitude at the fifth harmonic of the frequency spectrum. The magnitude at the fifth machine order from the frequency spectrum can then be used to estimate the strut-induced pressure amplitudes. Similarly, fluctuating pressure due to rotor/stator interaction can be estimated from the magnitude at the 37th machine order. The complete set of reduced data described in this paper for both the midspan and 85% span locations at flow coefficients of 0.48 and 0.54 is given in Ref. 8.

Strut-Induced Pressure Amplitudes

Since the primary concern is with the effect of the five downstream struts, a closer look at a fifth-harmonic data is needed. It is expected that some 5/rev signal may result from uncontrollable background disturbance, so test cases with no

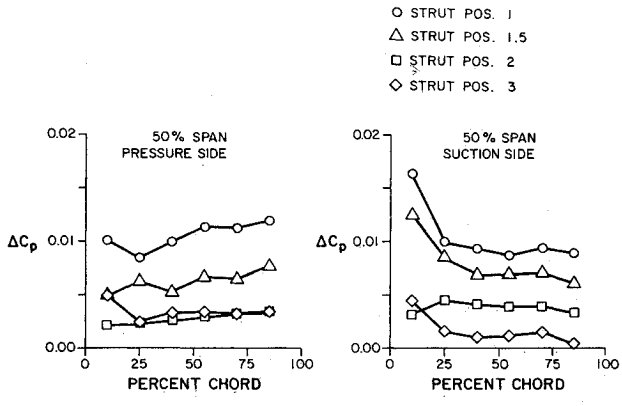

Fig. 4 Net unsteady pressure amplitudes due to strut, at the midspan and $C_x/U_T = 0.48$.

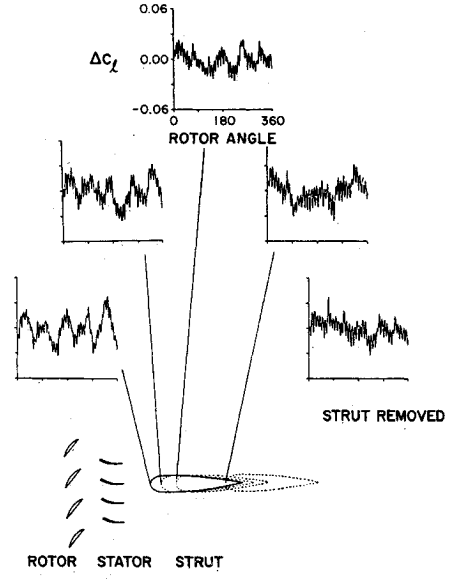

Fig. 5 Time-domain fluctuating lift coefficients at the midspan, $C_x/U_T = 0.48$.

struts are included for comparison. This no-strut component can be subtracted from those cases with struts to give *net* components due to the struts alone. However, a difference in phase must be accounted for. The Fourier transformation of the data produces a set of complex coefficients. They are converted to an amplitude and phase component at each frequency. The subtraction of the no-strut component is then done in the complex domain (vectorially).

Some typical data are shown in Fig. 4 for the midspan location of both the suction and pressure sides at a flow coefficient of 0.48. Trends of increasing pressure fluctuation level with a closer strut position are evident. With the struts at positions 1 and 1.5, the disturbance on the pressure side decreases from the trailing edge to the leading edge. This is expected, since the leading edge is farther upstream from the struts. However, this trend reverses on the suction surface and the first two transducers near the leading edge actually show a higher level of fluctuating pressure, as can be clearly seen in Fig. 2. The 5/rev disturbance on these two transducers is not uniform. It is possible that strut-induced flow separation on the suction surface leading edge can lead to such a behavior. Overall, the disturbance caused by the downstream struts is small, being only about 1% of the dynamic pressure.

Unsteady Lift and Moment Coefficients

A rotor blade experiences varying lift and moment as the surrounding pressure distribution changes. Unsteady lift ΔC_ℓ can be calculated by integrating the unsteady pressure over the blade surface. The unsteady moment ΔC_m calculation is similar and the moment arm is referenced to the blade quarter-chord. Again, only the unsteady component is presented.

A question arises concerning the precision of the six-point integration and the treatment of the leading and trailing edges. The integration is refined by using a 16 point spline fit across the chord. The pressures on the top and bottom blade surfaces are assumed to match at both the leading and the trailing edges. For spline fitting, that value is chosen midway between the nearest measured pressure and suction surface pressures.

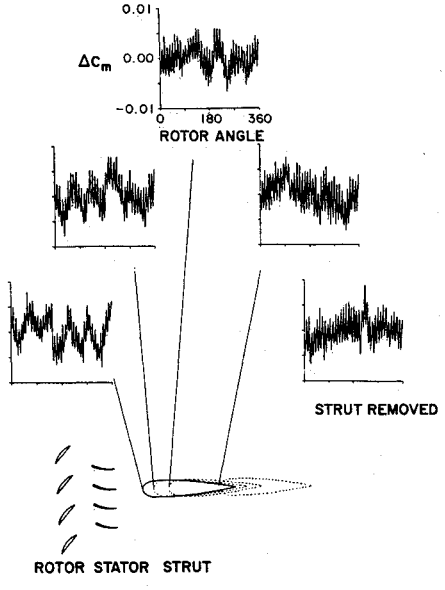

Fig. 6 Time-domain fluctuating moment coefficients at the midspan, $C_x/U_T = 0.48$.

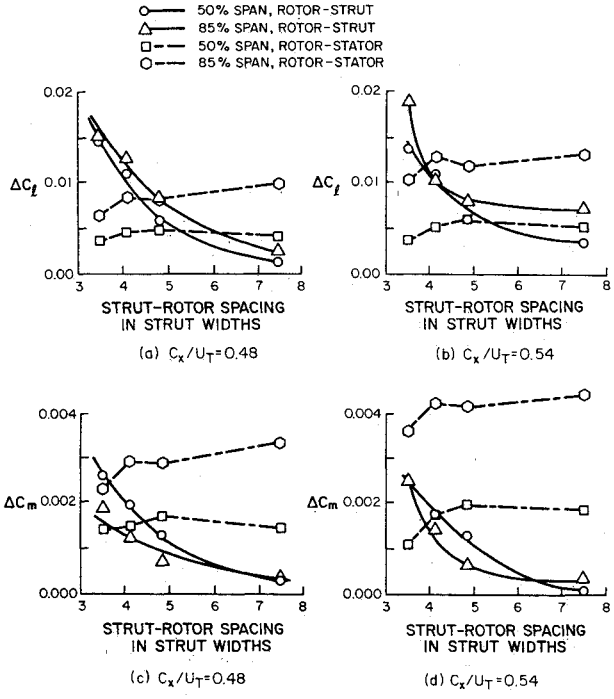

Fig. 7 Fluctuating lift and moment coefficients vs axial strut location.

The time-domain fluctuating lift data are shown in Fig. 5, which has five plots, one for each of the four strut locations tested and one for the data with the strut removed. The corresponding time-domain unsteady moment data are shown in Fig. 6. The data presented correspond to the midspan location and flow coefficient of 0.48. In each figure, the fluctuating coefficients are shown to the same scale. In Figs. 5 and 6, the rapid decay of the 5/rev disturbance with increasing rotor/strut distance can be readily seen. The 37/rev stator disturbance becomes quite dominant and periodic with the struts removed.

The frequency content of the unsteady lift and moment coefficients can be displayed by performing a digital Fourier transformation of data similar to that presented in Fig. 3. The corresponding unsteady lift and moment amplitudes at the 5th machine order (rotor/strut interaction) and 37th machine order (rotor/stator interaction) for different strut positions can be summarized. Figure 7 shows such data vs axial separation (nondimensionalized to strut thickness) measured from the rotor trailing edge to the strut leading edge. Figures 7a and 7b plot the unsteady lift coefficients for flow coefficients of 0.48 and 0.54, respectively, and Figs. 7c and 7d the corresponding unsteady moment coefficients. The data with the struts removed are essentially the same as the data for the case with the struts at position 3. Therefore, the data with the struts removed are not plotted. For clarity, experimental observations of the rotor/strut interaction will be presented first, followed by a discussion of rotor/stator interaction.

First, for the rotor/strut interaction (solid line in Fig. 7), the amplitudes are seen to decrease exponentially with increased strut axial separation from the rotor. The solid curves were fit with exponential functions of the form $y = \exp(a + bx)$. This observation is in agreement with an analytical model based on simple potential flow[3] in which the upstream pressure disturbance caused by a downstream body is predicted to decrease exponentially when the ratio of the upstream distance from the strut leading edge to strut thickness increases. For this reason, strut width is chosen to nondimensionalize the strut/rotor axial separation in Fig. 7. Second, from Fig 7, it is observed that the levels drop rapidly up to five strut thicknesses for both the unsteady lift and moment cases. The rate of dropoff becomes negligible at about six strut widths. There, given the available space, a 6 strut width spread between the rotor and strut would effectively reduce the rotor/strut interaction to insignificant levels, while 5 strut widths would reduce the interaction by over 50% from the design location of 3.5 widths.

A comparison of the midspan (solid line with symbol o) with the 85% span (solid line with symbol Δ) data in Fig. 7 for the rotor/strut interaction also reveals that there is only a very small difference in the absolute level of the unsteady lift and moment coefficients. In comparison, the midspan and 85% span curves basically follow the same trend. It is also apparent from Fig. 7 that the unsteady lift and moment caused by rotor/strut interaction is relatively independent of the flow coefficient.

An important observation is evident in these plots. The amplitude caused by rotor/strut interaction is not only in the same range as the rotor/stator interaction, but it exceeds the rotor/stator interaction at the design strut location (3.5 strut thicknesses). However, the magnitude of the strut effect falls below the stator effect as the struts approach five strut thicknesses separation. This observation has an important implication. At the design rotor/stator/strut spacing, the unsteadiness caused by rotor/strut interaction is higher than that due to rotor/stator interaction. Therefore, regarding noise generation and aeromechanical fatigue, the interaction of fan rotor flow with downstream struts can potentially pose a greater threat than the rotor/stator interaction.

Figure 7 also summarizes the effects of the interaction between the rotor and stator at the 37th machine order (dashed

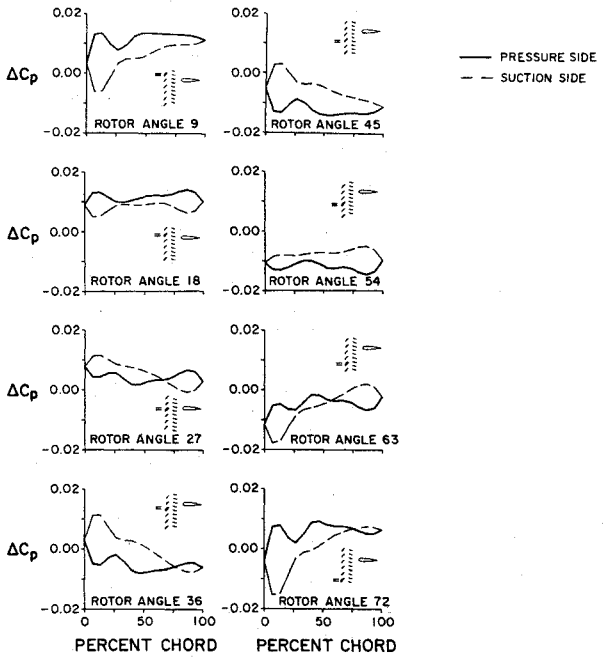

Fig. 8 Time series of pressure perturbation distribution plot at the midspan, $C_x/U_T = 0.48$, and strut at location 1.

line in Fig. 7) as follows:

1) Comparing the difference in the unsteady lift and moment coefficients for C_x/U_T of 0.48 and 0.54, little difference is seen at the 85% span location (dashed line with symbol ○). However, at the midspan (dashed line with symbol □), it is evident that the unsteady interaction is higher for a flow coefficient of 0.54. Previous investigation on rotor/stator interaction[9] with blade-mounted pressure transducers on the *stator blade* has shown that the unsteady lift coefficient on the stator decreases with increased C_x/U_T. At a higher flow coefficient, the incidence angle to the rotor is decreased and the loading on the rotor blades reduced. Hence, it is expected that a thinner wake will be shed from the rotor. This decrease in wake sizes leads to smaller fluctuation forces on the stator blade. However, in the present experiment, the upstream rotor blade is instrumented and the unsteady lift coefficient is measured on the rotor instead of on the stator. It is not clear how the unsteady lift coefficient on the rotor will change as the flow coefficient varies. It is possible that higher velocity can lead to greater upstream potential effects.

2) From Fig. 7, the rotor/stator unsteady interaction is observed to be relatively independent of the strut locations for strut positions 1.5, 2, and 3. However, with the strut at the most forward position (strut position 1), there is a notable decrease in the rotor/stator unsteady interaction. For example, at the design operation ($C_x/U_T = 0.48$) and at the 85% span location, the unsteady lift and moment coefficients both decrease by about 25% when the strut is moved from position 1.5 to 1. This decrease is smaller at the midspan, but becomes more significant at the higher flow coefficient for both spanwise locations.

3) Figure 7 shows there is significant three-dimensional effect between the rotor/stator interaction and, hence, future measurements should be made at more than one spanwise location.

Instantaneous Perturbation Pressure Distributions

In order to examine the effect of a particular frequency in the time domain, a digital bandpass filter was used to filter out all frequencies except for those of interest. This technique was used to retain the fifth harmonic for the instantaneous pressure distributions. This makes possible visual imaging of the perturbation effect caused by the downstream struts on the unsteady pressure distribution over the blade. The same perturbation pressure distribution appears every one-fifth revolution, which is every 72 deg.

A series of pressure perturbation distribution plots in time shows the progression of the downstream strut disturbance across the rotor blade chord. In Fig. 8, such a series is examined for the midspan location ($C_x/U_T = 0.48$) at strut location 1. The rotor angle is incremented by 9 deg from 9 to 72 deg, covering one complete strut passing (or one-fifth rotor revolution). The relative position of the rotor with respect to the strut for each corresponding angular position is also shown in Fig. 8. (The instrumented rotor blade is indicated by an = sign.) It is important to recall that the perturbation pressure is superimposed on the steady-state part and that what is being presented is only the fluctuating component. Looking more closely at Fig. 8, one can follow one cycle of the rotor as it passes one strut. At angle 9, the instrumented rotor blade is moving into the disturbance caused by the strut. At this angular position, the pressure side coefficient (solid line) exceeds the suction side coefficient (dashed line). Moving closer to the strut at angle 18, the suction side coefficient increases significantly, whereas the pressure side coefficient remains relatively unchanged, except for a slight increase near the leading edge. The high pressure levels on both surfaces at angle 18 indicate the peak of the disturbance, with the instrumented rotor blade moving close to a position directly upstream of the strut. Starting from angle 27, the instrumented rotor blade is moving away from the disturbance. Here, it is observed that the fluctuating pressure on the pressure side falls below that on the suction side, starting with the leading edge and moving along the chord. At both angles 27 and 36, the leading edge of the suction surface sees the maximum disturbance. At angles 45 and 54, the suction side fluctuating pressure completely exceeds that of the pressure side. The blade is between two adjacent struts at about angle 54 when the pressures are low on both sides. Starting from angle 63, the blade is moving into the next strut disturbance. Here, the pressures start to rise on both sides. At the leading edge, the fluctuating pressure on the pressure side exceeds that on the suction side. The pressure wave moves back along the chord on the pressure side, followed by increased pressure on the pressure side at angles 72 and 9. Then, a new cycle begins with rotor angle 9. Notice how the whole distribution rises and falls, reaching a maximum at angle 18 and a minimum at angle 54.

Results of Stationary Pressure Measurements

During the preliminary tests, it was determined that the probe located at 6.4 mm upstream of the rotor (probe A, Fig. 1) could not discriminate any flow distortion caused by the downstream struts. After conducting a radial traverse to determine the velocity profile in front of the rotor, measurements with that probe were abandoned. The radial profiles of total and static pressures were found to be uniform outside the hub and tip casing boundary layers.

Samples of the data from the probe measurements behind the rotor (probe B) and near the strut leading edge (probe C) are presented in Fig. 9. The data correspond to the midspan location and a flow coefficient of 0.48, with the strut in its most forward location (strut position 1). The data are typical in that for all other test cases, the circumferential distributions of flow quantities across one strut spacing follow the same trend, although the absolute d.c. level may differ somewhat. Figure 9 shows that the variation in flow angle measured by probe C is as much as 30 deg across the strut and C_{p_s} also increases by a factor of two. However, at a location 113 mm upstream from the leading edge of the strut (probe B), the variations reduced significantly. As expected, the total pressure coefficient at the rotor exit is higher than near the strut leading edge, since losses will occur through the stator blade row.

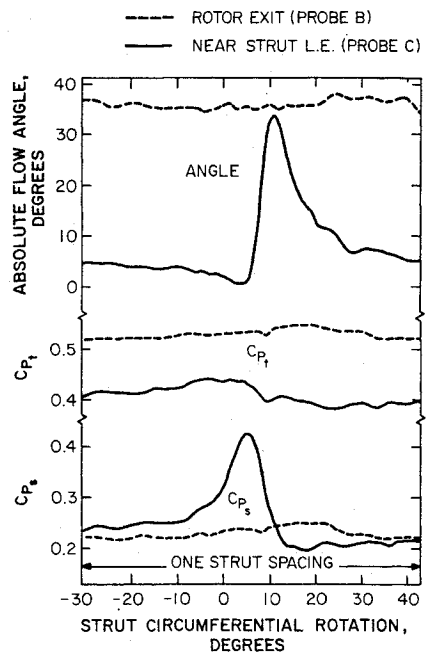

Fig. 9 Flow characteristics for strut location 1 at the midspan.

In order to compare the aerodynamic efficiency of the rotor with and without the presence of the downstream struts, the measurements at rotor exit from probe B were circumferentially area averaged between one strut spacing. The results are presented in Table 2.

The circumferential area averaging allows for a comparison of the overall aerodynamic efficiency of the rotor. This average is useful since the circumferential variations in flow quantities at the rotor exit are relatively small and basically follow the same trend. From Table 2, it can be seen that, even with the struts at the most forward position, the aerodynamic efficiency of the rotor, as indicated from pneumatic measurements, is not affected. This does not mean that the rotor does not see the strut at all. The magnitude of the disturbance is of acoustic level (small perturbation) and it hardly changes the efficiency of the rotor. Thus, the presence of the downstream struts has little or no measurable effect on the aerodynamic efficiency of the rotor. It is possible that the stator row is providing some screening effect and reduces the distortion at the rotor. In addition, the pneumatic probe may not be sensitive enough to measure the acoustic disturbance caused by the strut at the rotor exit.

Finally, it should be noted from Table 2 that, as the flow coefficient increases, the incidence angle to the rotor decreases and the aerodynamic loading on the rotor is reduced. As a result, the static pressure coefficient is about 10% less and the flow turning is also reduced by 4 deg.

In order to determine the change in the aerodynamic efficiency of the stator resulting from the presence of the downstream strut, it is necessary to measure flow quantities across the stator gap at the exit. This was not done in the experiment and, hence, it is not possible to draw any conclusion from the data set. However, it is expected that the blockage due to the strut can change the incidence angle at the stator. With reference to Fig. 1, it is seen that, because of strut blockage, the stator blade above the strut will see a decrease in the incidence angle, whereas the stator blade below will see the opposite effect. Further investigation is needed to determine the extent of the struts' influence on the aerodynamic performance of the stator.

Summary and Conclusions

The experiments have shown the nature and magnitude of the unsteady response of on-rotor pressures to the flow disturbances produced by the following stator blade row and also by the downstream struts. The effect of the upstream potential field of a strut row located on the rotor blade passage was shown to be larger than the stator effect at design rotor/stator/strut spacing. The magnitude of the unsteady pressure fluctuation on the rotor blade is about 1% of the dynamic pressure. Further investigation revealed an exponential relationship between rotor/strut interaction and axial spacing. The rotor/strut interaction decreases rapidly with an increase in axial separation between the rotor trailing edge and the strut leading edge, thereby decreasing the noise level and the possibility of rotor fatigue. The potential effect caused by the struts becomes neglibible after an axial separation of six strut thicknesses is reached. In addition, a technique has been developed to visualize rotor blade pressure distributions as they change with the rotor angle over time. The flow disturbance resulting from the strut can be seen to propagate down the chord as the blade passes through the disturbance.

Stationary pressure probe measurements show that the presence of the downstream struts can produce large variation in flow quantities near the strut leading edge. A flow angle change of about 30 deg was measured and the static pressure coefficient also increases by a factor of two across the strut. However, these variations are reduced significantly near the rotor trailing edge. The presence of the downstream strut has measurable effect on the aerodynamic efficiency of the rotor. Flow turning and the total and static pressure coefficients measured with pneumatic probe at the rotor exit remain unchanged with or without the struts.

Current effort is being directed toward developing an analytical model for the rotor/stator/strut interaction. This experimental program will be used to validate the analytical studies.

Acknowledgments

This work was supported by NASA Langley Research Center Applied Acoustics Branch, Mr. David Chestnutt, Branch Chief. Technical monitor for the grant was Mr. James A. Schoenster.

References

[1]Rubbert, P.E., Boctor, M.L., Cowan, S.J., and LaPrete, R.D., "Concept and Design of Stators Tailored to Shield a Fan from Pressure Disturbances Arising in the Downstream Fan Duct," AIAA Paper 72-84, Jan. 1972.

[2]Barber, T.J. and Weingold, H.D., "Vibratory Forcing Functions Produced by Nonuniform Cascades," *Transactions ASME, Journal of Engineering for Power*, Vol. 100, Jan. 1978, pp. 82-88.

[3]O'Brien, W.F., Ng, W.F., and Richardson, S.M., "Calculation of Unsteady Fan Rotor Response Caused by Downstream Flow Distortions," *Journal of Propulsion and Power*, Vol. 1, Nov.-Dec. 1985, pp. 464-469.

[4]Preisser, J.S., Schoenster, J.A., Golub, R.A., and Horne, C., "Unsteady Fan Blade Pressure and Acoustic Radiation from a JT15D-1 Turbofan Engine at Simulated Forward Speed," AIAA Paper 81-0096, Jan. 1981.

[5]Woodward, R.P. and Balombin, J.R., "Tone Generation by Rotor-Downstream Strut Interaction," *Journal of Aircraft*, Vol. 21, Feb. 1984, pp. 135-142.

[6]Yokoi, S., Nagano, S., and Kakehi, Y., "Reduction of Strut Induced Rotor Blade Vibration with the Modified Stator Setting Angles," *International Symposium on Airbreathing Engines*, 5th ed., Feb. 1981, pp. 61-1-61-7.

[7]Reimers, S.L., "An Investigation of Fan Flow Interaction with a Downstream Strut," M.S. Thesis, Dept. of Mechanical Engineering, Virginia Polytechnic Institute and State University, Blacksburg, 1983.

[8]Olsen, T.L., "Experimental Investigation of Unsteady Fan Flow Interaction with Downstream Struts," M.S. Thesis, Dept. of Mechanical Engineering, Virginia Polytechnic Institute and State University, Blacksburg, 1985.

[9]Gallus, H.E., Lambertz, J., and Wallmann, Th., "Blade-Row Interaction in an Axial-Flow Subsonic Compressor Stage," *Transactions of ASME, Journal of Engineering for Power*, Vol. 102, Jan. 1980, pp. 169-177.